Dynamic Analysis of a Three Phase 20HP, 400V, 50Hz Induction Machine Driven by A Hybrid Voltage Source Inverter under A Varying Machine Load.

C.O. OMEJE
Department of Electrical/Electronic Engineering, University of Port Harcourt, Rivers State Nigeria.

Abstract:
This paper evaluates a comprehensive analysis and a direct approach to induction machine dynamism. The mathematical modeling of the machine which helps to achieve its dynamic performance is presented herein. The effect of a varying mechanical load on the machine functionality and its characteristics impact on the speed and torque behaviour is also analyzed in this research work. Simulations were carried out on the modeled three phase asynchronous machine in MATLAB/SIMULINK 7.11 to show the transient and the steady state performance of the induction motor under a systemic fluctuating loading condition which emanates from an unsteady mechanical load applied on the machine. A direct control of induction machine is of great importance in terms of variable voltage and frequency. This control is easily realized with the aid of a power electronic device. Thus, a power semi-conductor device in the form of multilevel converter was employed as a source of a.c supply to the machine. This a.c supply is obtained from a hybrid five level voltage source inverter which is formed by a cascade of three level flying capacitor and H-bridge inverter using space vector pulse width modulation technique (**SVPWM**) for obvious harmonic reduction and efficient voltage profile. This technique was compared with the conventional multi-carrier sinusoidal method of pulse-width modulation (**SPWM)** to differentiate the efficiency level of the two modulation schemes.

Keyword: Induction Machine, Dynamic Equations, Multi-Level Converter, Multi-carrier Sinusoidal Pulse width modulation, Space Vector Modulation and Simulations.

1 INTRODUCTION

Induction machines or asynchronous machines are the most widely used machineries in most industries. The induction motors with squirrel-cage rotors serve as the work-horse or prime-mover of industrial appliances because of their low maintenance cost, robustness, high reliability, greater efficiency and good self-starting capability [1]-[2]. They are comparatively less expensive to equivalent size of a synchronous machine or d.c machines and range in sizes from a few watts to ten thousand horse power (7460Kilowatts) [3]. However, their speeds are not as easily controlled as the d.c motors. Three phase induction machines are called asynchronous speed machine because it can operate below or above its synchronous speed. When operating below its synchronous speed with positive slip value less than unity, it is said to be in its motoring mode while above the synchronous speed operation with negative slip value less than zero, it is known to be in its generating mode [3]. They draw large starting current which is about six to eight times their full load values and operate with a poor lagging power factor when lightly loaded [4]. However, speed and torque control of induction machine is attainable with power electronic devices. Thus, by direct application of power electronic converter as a source of machine supply, it is possible to vary and control the speed and torque of an induction machine as reflected in [5]. Analysis on the dynamic performance of a

modeled induction machine driving a constant external load using space vector modulated inverter source has been presented in [6]-[7] with no emphasis on the characteristic behaviour of the machine speed and torque under a varying loading condition. Similarly, the dynamic modeling and simulation of a 3-HP asynchronous motor with direct online starting method though driving a mechanical load was presented in [8] but had no reference to power electronics control and harmonic reduction to the machine stator supply or comparative advantage of the two modulation techniques as applied in this work. In [9], a seven-level inverter topology for induction motor drive using two-level inverters and floating capacitor fed H-bridges was presented. It is observed that at a frequency of 50Hz, the inverter operates at over modulation mode thus introducing a lower order harmonic into the machine stator which is unacceptable. The speed control of space vector modulated inverter driven induction motor was also reported in [10]. The results presented in this report only considered a step response in speed and a restricted inverter level to two level thus producing reduced fundamental phase and line voltage values which do not fit well into higher voltage magnitude application. This paper therefore presents a complete simulation study of asynchronous machine behaviour under a varying loading condition with respect to stator voltage harmonic reduction using multilevel converter space vector pulse width modulation which has a 1.15% voltage magnitude increase when compared to the conventional sinusoidal pulse width modulation thus increasing the dc bus voltage utilization [11].

To achieve the aforementioned objective, it is most convenient to simulate the machine and the power converter on a stationary reference frame in preference to the rotor and synchronously rotating reference frame.

2 MATHEMATICAL MODELING OF ASYNCHRONOUS MACHINE

The mathematical modeling applied in the simulation of induction machine were derived from the compilations proposed in [12].

Stator Voltage Equations in **abc** arbitrary reference frame are given by: (1)-(3).

$$V_{as} = i_{as}\, r_s + \frac{d\lambda_{as}}{dt} \quad \text{(volts)} \qquad (1)$$

$$V_{bs} = i_{bs}\, r_s + \frac{d\lambda_{bs}}{dt} \quad \text{(volts)} \qquad (2)$$

$$V_{cs} = i_{cs}\, r_s + \frac{d\lambda_{cs}}{dt} \quad \text{(volts)} \qquad (3)$$

Rotor Voltage Equations in **abc** arbitrary reference frame are given by: (4)-(6).

$$V_{ar} = i_{ar}\, r_r + \frac{d\lambda_{ar}}{dt} \quad \text{(volts)} \qquad (4)$$

$$V_{br} = i_{br}\, r_r + \frac{d\lambda_{br}}{dt} \quad \text{(volts)} \qquad (5)$$

$$V_{cr} = i_{cr}\, r_r + \frac{d\lambda_{cr}}{dt} \quad \text{(volts)} \qquad (6)$$

Flux linkage equations in **abc** arbitrary reference frame are given by: (7) -(11).

$$\begin{bmatrix} \lambda_s^{abc} \\ \lambda_s^{abc} \end{bmatrix} = \begin{bmatrix} L_{ss}^{abc} & L_{sr}^{abc} \\ L_{rs}^{abc} & L_{rr}^{abc} \end{bmatrix} \begin{bmatrix} i_s^{abc} \\ i_r^{abc} \end{bmatrix} \text{(Wb.turn)} \qquad (7)$$

Where:

$$\lambda_s^{abc} = (\lambda_{as}, \lambda_{bs}, \lambda_{cs})^t \qquad (8)$$

$$\lambda_r^{abc} = (\lambda_{ar}, \lambda_{br}, \lambda_{cr})^t \qquad (9)$$

$$i_s^{abc} = (i_{as}, i_{bs}, i_{cs})^t \qquad (10)$$

$$i_r^{abc} = (i_{ar}, i_{br}, i_{cr})^t \qquad (11)$$

The idealized three phase induction machine is assumed to have a symmetrical air gap. The **qdo**

arbitrary reference frame is usually selected on the basis of convenience and compatibility with the representations of other network components. The two common reference frames used in the analysis of induction machine are the stationary and synchronously rotating reference frames [12]. In the stationary rotating reference frame, the **dq** variables of the machine are in the same frame as those normally used for the supply network. This is a convenient choice of frame when the supply network is large or complex. In the synchronously rotating reference frame, the **dq** variables are always constant in steady state, thus forming a condition for driving a small signal model about a chosen operating point. In the stationary reference frame, the angular speed **ω** is always set to zero while in the synchronously rotating reference frame it is set to $\boldsymbol{\omega_e}$ [13].

The stator voltage equations in **qdo** arbitrary reference frame are given by: (12) -(16).

$$V_s^{qdo} = \omega \begin{bmatrix} 0 & 1 & 0 \\ -1 & 0 & 0 \\ 0 & 0 & 0 \end{bmatrix} \lambda_s^{qdo} + \rho\lambda_s^{qdo} + r_s^{qdo} i_s^{qdo} \quad (12)$$

Where: $\boldsymbol{\omega} = \frac{d\theta}{dt}$

$$r_s^{qdo} = r_s \begin{bmatrix} 1 & 0 & 0 \\ 0 & 1 & 0 \\ 0 & 0 & 1 \end{bmatrix} \quad (13)$$

$$V_s^{qdo} = (V_{qs}, V_{ds}, V_{os})^t \quad (14)$$

$$\lambda_s^{qdo} = (\lambda_{qs}, \lambda_{ds}, \lambda_{os})^t \quad (15)$$

$$i_s^{qdo} = (i_{qs}, i_{ds}, i_{os})^t \quad (16)$$

The rotor voltage equations in **qdo** arbitrary reference frame are given by: (17) -(21).

$$V_r^{qdo} = (\omega - \omega_r) \begin{bmatrix} 0 & 1 & 0 \\ -1 & 0 & 0 \\ 0 & 0 & 0 \end{bmatrix} \lambda_r^{qdo} + \rho\lambda_r^{qdo} + r_r^{qdo} i_r^{qdo} \quad (17)$$

Where: $\boldsymbol{\omega} = \frac{d\theta}{dt}$ and $\boldsymbol{\omega_r} = \frac{d\theta_r}{dt}$

$$r_r^{qdo} = r_r \begin{bmatrix} 1 & 0 & 0 \\ 0 & 1 & 0 \\ 0 & 0 & 1 \end{bmatrix} \quad (18)$$

$$V_r^{qdo} = (V_{qr}, V_{dr}, V_{or})^t \quad (19)$$

$$\lambda_r^{qdo} = (\lambda_{qr}, \lambda_{dr}, \lambda_{or})^t \quad (20)$$

$$i_r^{qdo} = (i_{qr}, i_{dr}, i_{or})^t \quad (21)$$

A modified stator and rotor flux linkage equations is compactly written in matrix form in terms of inductance as shown in (22).

$$\begin{bmatrix} \lambda_{qs} \\ \lambda_{ds} \\ \lambda_{os} \\ \lambda_{qr}^i \\ \lambda_{dr}^i \\ \lambda_{or}^i \end{bmatrix} = \begin{bmatrix} X & 0 & 0 & L_m & 0 & 0 \\ 0 & X & 0 & 0 & L_m & 0 \\ 0 & 0 & L_{LS} & 0 & 0 & 0 \\ L_m & 0 & 0 & Y & 0 & 0 \\ 0 & L_m & 0 & 0 & Y & 0 \\ 0 & 0 & 0 & 0 & 0 & L_{Lr}^i \end{bmatrix} \begin{bmatrix} i_{qs} \\ i_{ds} \\ i_{os} \\ i_{qr}^i \\ i_{dr}^i \\ i_{or}^i \end{bmatrix} (W - T) \quad (22)$$

Where $X = L_{LS} + L_m$ and $Y = L_{Lr}^i + L_m$

The induction machine equations in stationary reference frame are presented as follows:

$$V_{qs}^s = \frac{\rho}{\omega_b}\psi_{qs}^s + r_s i_{qs}^s \quad (23)$$

$$V_{ds}^s = \frac{\rho}{\omega_b}\psi_{ds}^s + r_s i_{ds}^s \quad (24)$$

$$V_{os} = \frac{\rho}{\omega_b}\psi_{os} + r_s\, i_{os} \quad (25)$$

$$V_{qr}^{is} = \frac{\rho}{\omega_b}\psi_{qr}^{is} - \frac{\omega_r}{\omega_b}\psi_{dr}^{is} + r_r^i\, i_{qr}^{is} \quad (26)$$

$$V_{dr}^{is} = \frac{\rho}{\omega_b}\psi_{dr}^{is} + \frac{\omega_r}{\omega_b}\psi_{qr}^{is} + r_r^i\, i_{dr}^{is} \quad (27)$$

$$V_{or}^{i} = \frac{\rho}{\omega_b}\psi_{or}^{i} + r_r^i\, i_{or}^{i} \quad (28)$$

Where: $\boldsymbol{\psi} = \boldsymbol{\omega_b\lambda}$, $\boldsymbol{\psi_{qs}} = \boldsymbol{\omega_b\lambda_{qs}}$, $\boldsymbol{\psi_{ds}} = \boldsymbol{\omega_b\lambda_{ds}}$, $\boldsymbol{\psi_{os}} = \boldsymbol{\omega_b\lambda_{os}}$, $\boldsymbol{\rho} = \frac{\mathbf{d}}{\mathbf{dt}}$, $\boldsymbol{\omega_b}$ is called base electrical angular velocity in rad./sec. Also, $\boldsymbol{\omega_b L_{LS}} = \mathbf{X_{LS}}$, $\boldsymbol{\omega_b L_m} = \mathbf{X_m}$, $\boldsymbol{\omega_b L_r^i} = \mathbf{X_{Lr}^i}$

A modified stator and rotor flux linkage equations are compactly written in matrix form in terms of reactance as shown in (29).

$$\begin{bmatrix} \psi_{qs}^s \\ \psi_{ds}^s \\ \psi_{os} \\ \psi_{qr}^{is} \\ \psi_{dr}^{is} \\ \psi_{or}^{i} \end{bmatrix} = \begin{bmatrix} A & 0 & 0 & X_m & 0 & 0 \\ 0 & A & 0 & 0 & X_m & 0 \\ 0 & 0 & X_{LS} & 0 & 0 & 0 \\ X_m & 0 & 0 & B & 0 & 0 \\ 0 & X_m & 0 & 0 & B & 0 \\ 0 & 0 & 0 & 0 & 0 & X_{Lr}^i \end{bmatrix} \begin{bmatrix} i_{qs}^s \\ i_{ds}^s \\ i_{os} \\ i_{qr}^{is} \\ i_{dr}^{is} \\ i_{or}^{i} \end{bmatrix} \quad (v-s) \quad (29)$$

Where $A = X_{LS} + X_m$ and $B = X_{Lr}^i + X_m$

The Electromechanical Torque equations are given by: (30) -(32)

$$T_{em} = \frac{3}{2}\frac{\rho}{2\omega_b}\left(\psi_{qr}^{is}\, i_{dr}^{is} - \psi_{dr}^{is} i_{qr}^{is}\right) (N.m) \quad (30)$$

$$T_{em} = \frac{3}{2}\frac{\rho}{2\omega_b}\left(\psi_{ds}^{s}\, i_{qs}^{s} - \psi_{qs}^{s} i_{ds}^{s}\right) (N.m) \quad (31)$$

$$T_{em} = \frac{3}{2}\frac{\rho}{2\omega_b} X_m\left(i_{dr}^{is}\, i_{qs} - i_{qr}^{is} i_{ds}^{s}\right) (N.m) \quad (32)$$

The above modeled equations are used in the simulation of a three-phase, **P**-pole, symmetrical induction machine in the stationary reference frame. The input/supply voltages to the stator terminal are obtained from the three phase output voltage of the hybrid five-level voltage source inverter topology.

For ease in simulation, the mathematical models of the induction machine in the stationary qdo reference frame are arranged into the following form:

$$\psi_{qs}^s = X_{LS}\, i_{qs}^s + \psi_{mq}^s \quad (33)$$

$$\psi_{mq}^s = X_m\left(i_{qs}^s + i_{qr}^{is}\right) \quad (34)$$

$$\psi_{ds}^s = X_{LS}\, i_{ds}^s + \psi_{md}^s \quad (36)$$

$$\psi_{qr}^{is} = X_{Lr}^i\, i_{qr}^{is} + \psi_{mq}^s \quad (37)$$

$$\psi_{dr}^{is} = X_{Lr}^i\, i_{dr}^{is} + \psi_{md}^s \quad (38)$$

$$i_{qs}^s = \frac{\psi_{qs}^s - \psi_{mq}^s}{X_{LS}} \quad (39)$$

$$i_{ds}^s = \frac{\psi_{ds}^s - \psi_{md}^s}{X_{LS}} \quad (40)$$

$$i_{qr}^{is} = \frac{\psi_{qr}^{is} - \psi_{mq}^s}{X_{Lr}^i} \quad (41)$$

$$i_{dr}^{is} = \frac{\psi_{dr}^{is} - \psi_{md}^s}{X_{Lr}^i} \quad (42)$$

Substitution of equations (39) -(42) into equations (23) -(28) with flux-linkages made subject of the formula gives rise to a modified flux-linkage equations presented in (43) -(52).

$$\psi_{qs}^s = \omega_b \int \left\{ V_{qs}^s + \frac{r_s}{X_{Ls}}\left(\psi_{mq}^s - \psi_{qs}^s\right)\right\} dt \quad (43)$$

$$\psi_{mq}^s = X_M\left(\frac{\psi_{qs}^s}{X_{Ls}} + \frac{\psi_{qr}^{is}}{X_{Lr}^i}\right) \quad (44)$$

$$\psi_{ds}^s = \omega_b \int \left\{ V_{ds}^s + \frac{r_s}{X_{Ls}}\left(\psi_{md}^s - \psi_{ds}^s\right)\right\} \quad (45)$$

$$\psi_{md}^s = X_M\left(\frac{\psi_{ds}^s}{X_{Ls}} + \frac{\psi_{dr}^{is}}{X_{Lr}^i}\right) \quad (46)$$

$$\frac{1}{X_M} = \frac{1}{X_m} + \frac{1}{X_{Ls}} + \frac{1}{X_{Lr}^i} \quad (47)$$

$$i_{os} = \frac{\omega_b}{X_{Ls}} \int \{V_{os} - r_s\, i_{os}\}\, dt \quad (48)$$

$$\psi_{qr}^{is} = \omega_b \int \left\{ V_{qr}^{is} + \frac{\omega_r}{\omega_b} \psi_{dr}^{is} + \frac{r_r^i}{X_{Lr}^i} \left(\psi_{mq}^s - \psi_{qr}^{is} \right) \right\} dt \quad (49)$$

$$\psi_{dr}^{is} = \omega_b \int \left\{ V_{dr}^{is} - \frac{\omega_r}{\omega_b} \psi_{qr}^{is} + \frac{r_r^i}{X_{Lr}^i} \left(\psi_{md}^s - \psi_{dr}^{is} \right) \right\} dt \quad (50)$$

$$i_{or}^i = \frac{\omega_b}{X_{Lr}^i} \int \{ V_{or}^i - r_r^i i_{or}^i \} dt \quad (51)$$

The equation of motional torque for the rotor axis is obtained by equating the inertia torque to the accelerating torque as depicted in (52).

$$J \frac{d\omega_{rm}}{dt} = T_{em} + T_{mech} - T_{damp} \ (N.m) \quad (52)$$

T_{mech} is the externally applied mechanical torque in the direction of the rotor speed and T_{damp} is the damping torque which is in the direction opposite to the rotation of the rotor [13].

$$T_{damp} = B\omega_m \quad (N.m) \quad (53)$$

Where B = coefficient of viscosity or damping coefficient (N.M.S).

The per unit speed $\frac{\omega_r}{\omega_b}$ needed for building the speed voltage terms in the rotor voltage equations can be obtained by integrating equation (54) while its dynamic characteristic is plotted in figure 4.6.

$$\frac{2J\omega_b}{p} \frac{d\left(\frac{\omega_r}{\omega_b}\right)}{dt} = T_{em} + T_{mech} - T_{damp} \ (N.m) \quad (54)$$

Most often, equation (54) is written in terms of the inertia constant **H** which is defined as the ratio of the kinetic energy of the rotating mass at base speed to the actual rated power. This gives rise to (55).

$$H = \frac{J\omega_b^2}{2S_b} \quad (55)$$

Expressing (55) in per unit values of the machine's base power and voltage gives rise to (56)

$$2H \frac{d\left(\frac{\omega_r}{\omega_b}\right)}{dt} = T_{em} + T_{mech} - T_{damp} \ (N.m) \quad (56)$$

The value of the externally applied mechanical torque T_{mech} is produced using a repeating sequence block obtained from the source block in the SIMULINK sub-library. This value of T_{mech} is varied from negative to positive so as to determine the motoring and generating characteristics of the motor as indicated in the preceding simulation plot presented in figure 20 while the simulation parameter used is presented in table 1.0. The dynamic equivalent circuit of the induction machine is shown in figure 1.0.

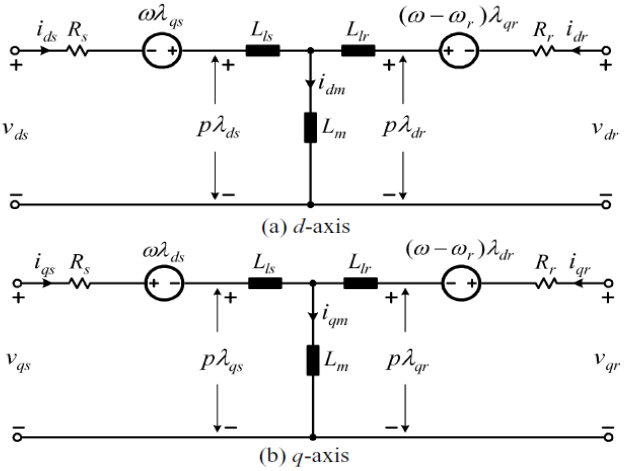

Figure 1.0 Dynamic Equivalent Circuit of an Induction motor.

TABLE 1.0: SIMULATION PARAMETERS FOR THE 20HP INDUCTION MOTOR.

MACHINE PARAMETERS	PARAMETER VALUES
RATED POWER (kW)	14.92
RATED PHASE/SUPPLY VOLTAGE (VOLTS)	400
STATOR RESISTANCE (Ω)	0.2
ROTOR RESISTANCE (Ω)	0.4
STATOR LEAKAGE INDUCTANCE (H)	0.04775
ROTOR LEAKAGE INDUCTANCE (H)	0.04775

MAGNETISING INDUCTANCE (H)	0.0955
NUMBER OF POLE PAIR	2
FREQUENCY (HERTZ)	50
SYNCHRONOUS SPEED (RPM)	1500
COEFFICIENT OF VISCOSITY/DAMPING COEFFICIENT (Nms)	0.0008
MOTOR INERTIA (Kg-m^2)	0.025

Figure 1.0 shows a typical closed-loop speed control scheme which uses volts/hertz and slip regulation method. The major blocks consist of a d.c supply and pulse width modulated signal supplied to the proposed inverter, a three phase five-level pulse width modulated inverter, an RC low pass filter and a 20HP, 400volt induction motor with externally applied mechanical torque and output speed in Rad/Sec.

The speed loop generates the slip speed via the proportional-integral controller of values of 1 and 0.005. The resultant speed is summed up to produce the desired motor speed which is converted to produce a varied supply frequency corresponding to a varied motor speed to the proposed five-level inverter with the aid of Simulink feed-back (closed loop) gain-block as shown in figure 3.0

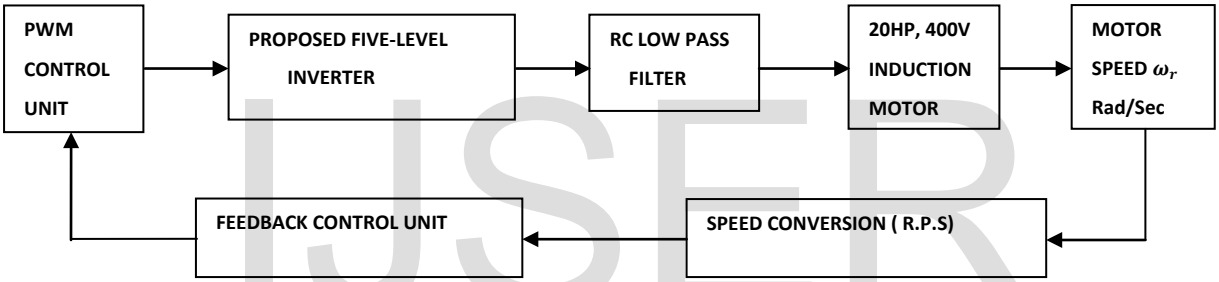

Figure 2.0: Block Diagram of the Closed Loop Inverter Fed Induction Motor.

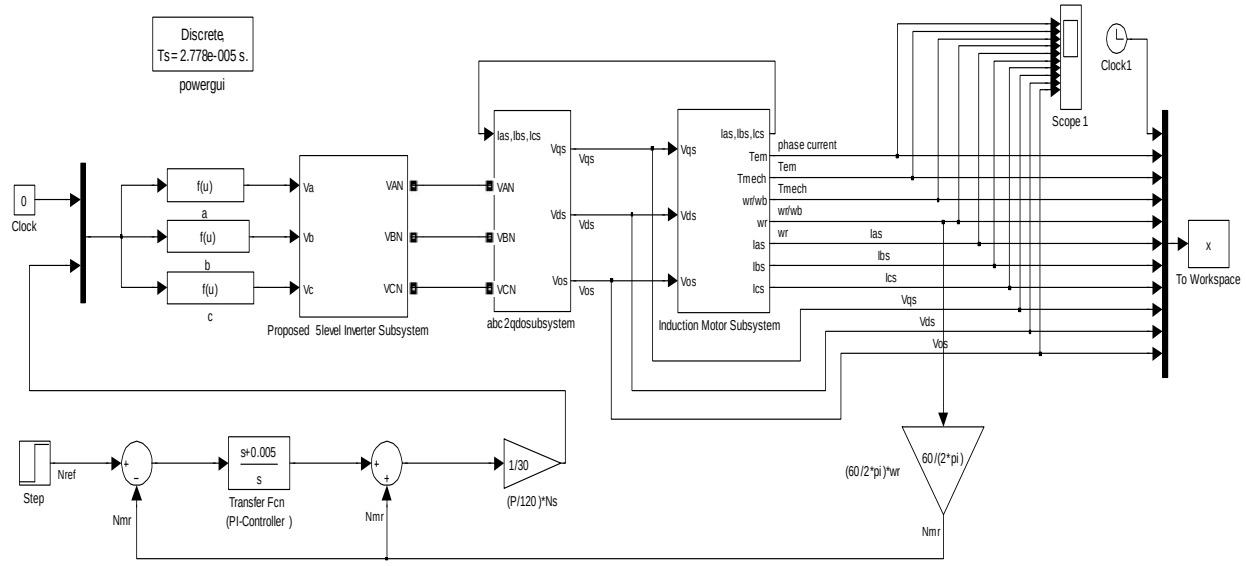

Figure 3.0: Simulink Diagram of the Closed Loop Inverter Fed Induction Motor with V/F System.

3.0 Multi-level Converter and Multi-Carrier Sinusoidal Pulse-Width Modulation.

In the proposed five-level topology, the In-phase disposition modulation scheme **(IPD)** was adopted. The realization of this scheme was done by comparing the modulating /reference signal at the fundamental frequency value with four triangular carrier waves having higher switching frequency than the modulating signal and in phase with it but with different offset voltage values. The carrier to fundamental frequency ratio or the frequency modulation index for this topology was adopted to be $\frac{5000}{50} = \mathbf{100}$ for better performance of the proposed multi-level PWM.

The operational principles of the proposed five-level inverter can be explained as follows:

For one cycle of the fundamental frequency, the proposed multilevel operates through four (4) different modes as illustrated in figure 4.0

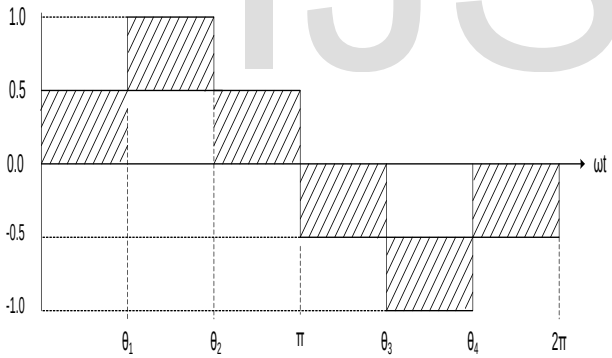

Figure 4.0: Modes of Voltage Level in a Cycle.

Mode 1: $0 \leq \omega t \leq \theta_1$ and $\theta_2 \leq \omega t \leq \pi$

Mode 2: $\theta_1 \leq \omega t \leq \theta_2$

Mode 3: $\pi \leq \omega t \leq \theta_3$ and $\theta_4 \leq \omega t \leq 2\pi$

Mode 4: $\theta_3 \leq \omega t \leq \theta_4$

The switching process varies comparatively with these four modes and the corresponding modulation index.

For $M_a \leq 0.5$, $0 \leq \omega t \leq \theta_1$ and $\theta_2 \leq \omega t \leq \pi$. T_3 is compared with the reference signal to produce a firing pulse for s_{a1} of the three-level flying capacitor cascaded to H-bridge inverter.

For $M_a \leq 1.0, \theta_1 \leq \omega t \leq \theta_2$. T_4 is compared with the reference signal to produce a triggering pulse for s_{a3} of the H-bridge cascaded to the three-level flying capacitor.

For $M_a \leq -0.5, \pi \leq \omega t \leq \theta_3$ and $\theta_4 \leq \omega t \leq 2\pi$. T_2 is compared with the reference signal to produce a firing pulse for s_{a2} of the three-level flying capacitor cascaded to H-bridge inverter.

For $M_a \leq -1.0$, $\theta_3 \leq \omega t \leq \theta_4$. T_1 is compared with the reference signal to produce a triggering pulse for s_{a4} of the H-bridge cascaded to the three-level flying capacitor.

Conversely, $\overline{S_{a1}}, \overline{S_{a2}}, \overline{S_{a3}}$ and $\overline{S_{a4}}$ switches are complementary to s_{a1}, s_{a2}, s_{a3} and s_{a4}. They are respectively fired by the corresponding logical switching functions shown in table 2. Figure 5.0 represents the eight switching pulses produced at phase A when the four carrier signals are compared with the reference or modulating wave. It is observed from figure 5.0 that the two inner triangular waves T_3 and T_2 are used to control the modulation of the three-level flying capacitor while the remaining two outer triangular waves T_4 and T_1 are used to control the modulation of the H-bridge cascaded with the three-level flying capacitor inverter.

The triangular carrier waveforms used in this modulation were assigned the following offset voltage values during the modulation process:

$$\left.\begin{matrix} T_3 = [0 \quad 0.5 \quad 0] \\ T_2 = [-0.5 \quad 0 \quad -0.5] \end{matrix}\right\}$$ Triangular carrier off set value for the 3-level FCC inverter

$$\left.\begin{matrix} T_4 = [0.5 \quad 1 \quad 0.5] \\ T_1 = [-1 \quad -0.5 \quad -1] \end{matrix}\right\}$$ Triangular carrier off set value for the H-bridge cascaded inverter

The sinusoidal equations used as a modulating signal for the reviewed three phases, multi-level converters are presented as follows:

$$V_{AN} = \frac{1}{\sqrt{3}} \times V_{LL} \times \sin \omega t \quad (57)$$

$$V_{BN} = \frac{1}{\sqrt{3}} \times V_{LL} \times \sin\left(wt - \frac{2\pi}{3}\right) \quad (58)$$

$$V_{CN} = \frac{1}{\sqrt{3}} \times V_{LL} \times \sin\left(wt - \frac{4\pi}{3}\right) \quad (59)$$

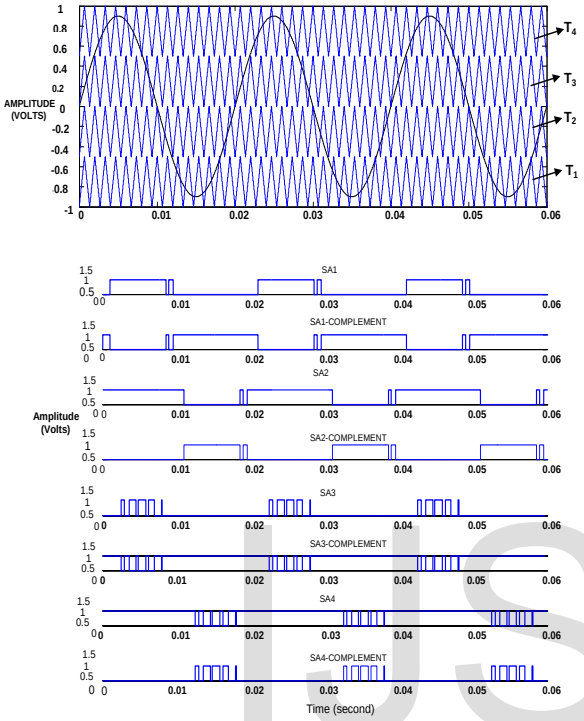

Figure 5.0: Eight Switching Signals for the Proposed Five-Level Topology Using SPWM.

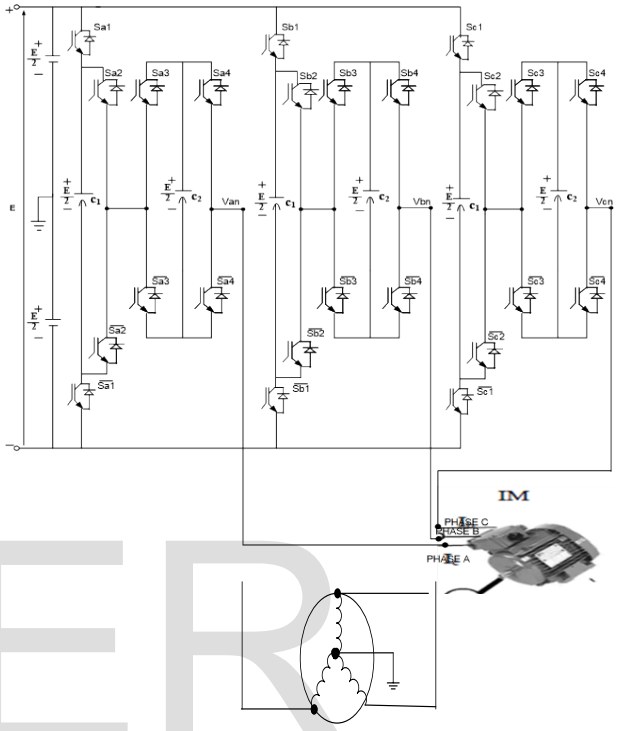

Figure 6.0: Circuit Diagram of the Proposed Five Level Inverter Topology.

Table 2.0: Switching Sequence and Output Voltages of the Proposed Five-Level Topology.

s_{a1}	s_{a2}	s_{a3}	s_{a4}	$\overline{S_{a1}}$	$\overline{S_{a2}}$	$\overline{S_{a3}}$	$\overline{S_{a4}}$	V_{an}	C_1 ia>0	C_1 ia<0	C_2 ia>0	C_2 ia<0	
1	1	0	1	0	0	1	0	E	*	*	-	+	
1	1	1	1	0	0	0	0	$E/2$	*	*	*	*	Positive Half-Cycle
1	1	0	0	0	0	1	1	$E/2$	*	*	*	*	
1	1	1	0	0	0	0	1	0	*	*	+	-	
1	0	1	1	0	1	0	0	0	+	-	*	*	
1	0	0	0	0	1	1	1	0	+	-	*	*	
0	1	1	1	1	0	0	0	0	-	+	*	*	
0	1	0	0	1	0	1	1	0	-	+	*	*	
0	0	0	1	1	1	1	0	0	*	*	-	+	
0	0	1	1	1	1	0	0	$-E/2$	*	*	*	*	Negative Half-Cycle
0	0	0	0	1	1	1	1	$-E/2$	*	*	*	*	
0	0	1	0	1	1	0	1	-E	*	*	+	-	

Key Notation : * denotes no effect, + denotes Charging, - denotes discharging.

4.0 Basic Concept of Space Vector Pulse Width Modulation

Space vector pulse width modulation (SVPWM) is a modulation technique that involves the generation of a reference vector (V_{ref}) representing a three phase sinusoidal voltage realized by switching between two nearest active vectors and one zero vector switching sequence of a given power converter [14]. In this work, this modulation technique is compared with a third harmonic injection to the conventional SPWM at modulation index of 0.8 to verify its similarity with SVPWM at one-sixth of SPWM fundamental value as reported in [14]. Over-modulation which occurs when the amplitude modulation index (m_a) is greater than unity is not considered since it causes a reduction in the number of pulses produced in the line-line voltage (V_{AB}) waveform leading to the emergence of low-order harmonics such as the 5^{th} and 11^{th} harmonics. The over-modulation is rarely used in practice due to the difficulties in filtering out the low order harmonics as well as the non-linear relationship between V_{AB} and m_a.

The basic idea of space vector pulse width modulation is to compensate for the dv/dt losses and undue harmonic distortions obtained using a SPWM technique and their corresponding on time. From reliable literature material, space vector PWM control can be realized by these steps:

- Step 1. Determine the reference voltage (Vref.) and its rotation angle ($\boldsymbol{\theta_0}$).
- Step 2. Determine the on-time for the zero vector and the two active vectors that is t_o, t_a, t_b, using the two nearest adjacent active voltage vectors and zero vector such as V_a, V_b and V_o otherwise known as the nearest three vectors concept.
- Step 3. Determine the possible switching patterns at every sector (S_1 to S_6) as Vref rotates across sectors (S_1-S_6) [14].

To determine the duty-cycle and switching on time of a Multilevel SVPWM inverter, the switching sequence of sector-one in figure 7 is applied in determining the switching time for the two active and zero vectors [15].

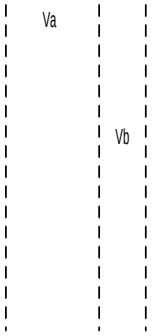

Figure 7: Half Cycle Switching Sequence of Two Active and a Zero Vector.

The best possible PWM pattern for each switching period in space vector modulation is achieved by applying a zero vector followed by two adjacent active state vectors in half switching period. The next half of the switching period is the mirror image of the first half. Therefore, integrating over a half cycle switching period, the time relating to each voltage vector in figure 7 is calculated as follows:

$$\int_0^{\frac{T_s}{2}} V_{ref}.\,dt = \int_{\frac{T_0}{2}}^{\frac{T_a}{2}+\frac{T_0}{2}} V_a.\,dt + \int_{\frac{T_a}{2}+\frac{T_0}{2}}^{\frac{T_b}{2}+\frac{T_a}{2}+\frac{T_0}{2}} V_b.\,dt \quad (60)$$

$$V_{ref} \times \frac{T_s}{2} = V_a\left(\frac{T_a}{2}+\frac{T_0}{2}-\frac{T_0}{2}\right) + V_b\left(\frac{T_b}{2}+\frac{T_a}{2}+\frac{T_0}{2} - \left(\frac{T_a}{2}+\frac{T_0}{2}\right)\right) \quad (61)$$

$$V_{ref} \times \frac{T_s}{2} = V_a \times \frac{T_a}{2} + V_b \times \frac{T_b}{2} \quad (62)$$

$$V_{ref} = V_a \times \frac{T_a}{T_s} + V_b \times \frac{T_b}{T_s} \quad (63)$$

The arrangement of these switching on-times in the six sectors of the multi-level inverter is achievable with the aid of the seven segment switching sequence as the reference vector rotates across each sector. The switching sequence for the three phase multi-level inverter in each of the six sectors are elaborately presented in figure 8 with **0** representing a switched off mode or zero output voltage and **P = 1** represents a switched on mode or positive terminal output voltage.

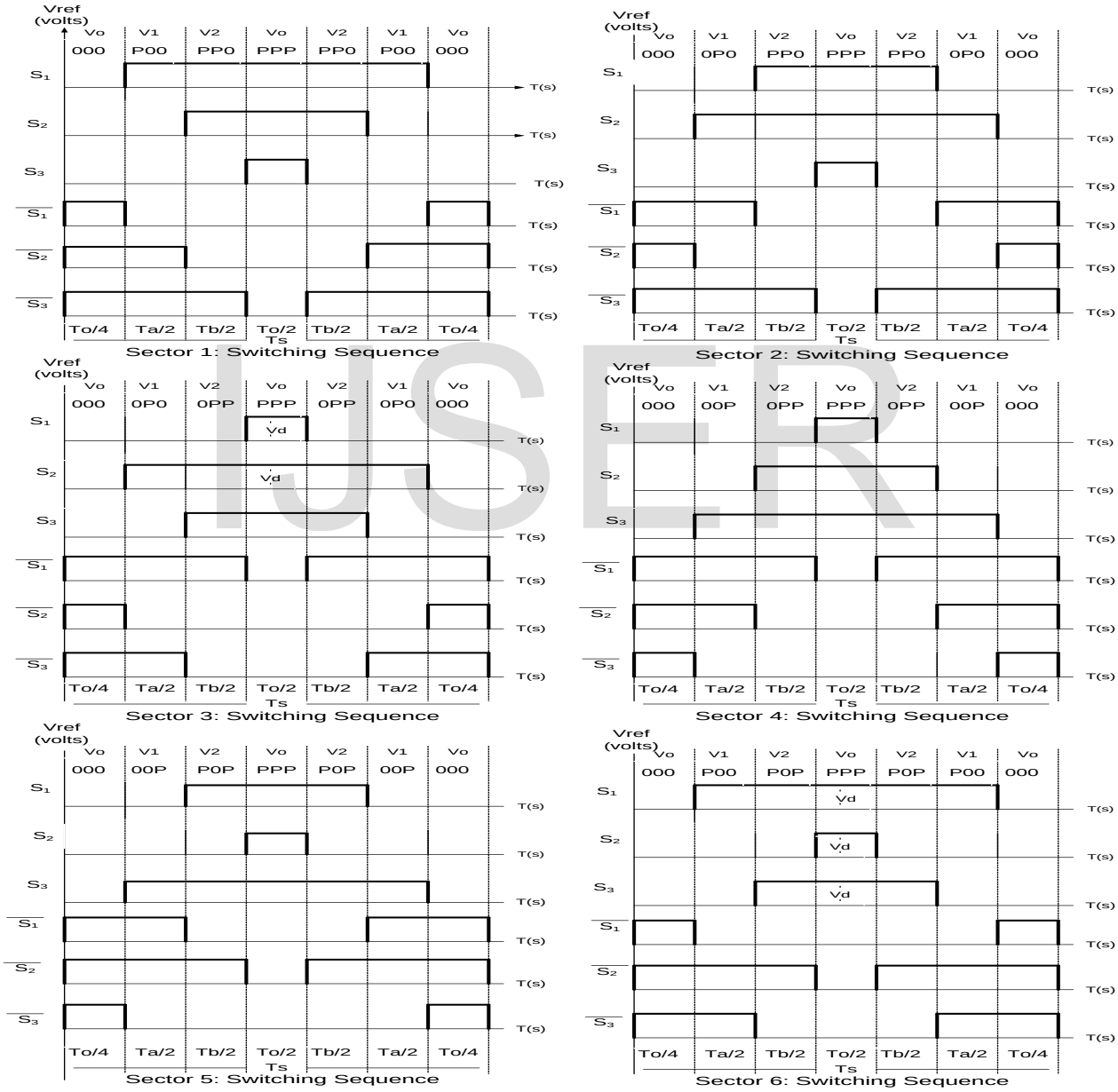

Figure 8: Space Vector Switching Sequence in Sectors 1-6

The above seven segments switching sequence for the six sectors are tabulated as follows:

Table 3: Seven Segments Switching Sequence of Six Sectors

Sector	V_0	V_1	V_2	V_0	V_2	V_1	V_0
I	000	P00	PP0	PPP	PP0	P00	000
II	000	0P0	PP0	PPP	PP0	0P0	000
III	000	0P0	0PP	PPP	0PP	0P0	000
IV	000	00P	0PP	PPP	0PP	00P	000
V	000	00P	P0P	PPP	P0P	00P	000
VI	000	P00	P0P	PPP	P0P	P00	000

The five-level voltage states distribution in the six sectors is presented in sextant form as shown:

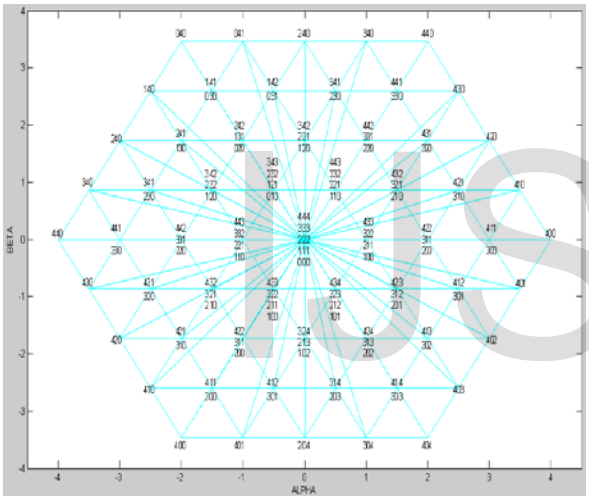

Figure 9: Sextant Diagram for Five-Level Inverter

In figure 9, there are 61 states of voltage vector locations possible for the five-level space vector structure. Most of these voltage vector locations which are about 37 have redundant switching state combination that are effectively used in PWM control to minimize the inverter switching transitions.

The rotation of the reference vector along the five-level region in sectors 1 and 2 is presented in figure 10 while sector 2 is a reversal of sector 1 with a shift in the rotation angle of the reference vector beyond 60^0.

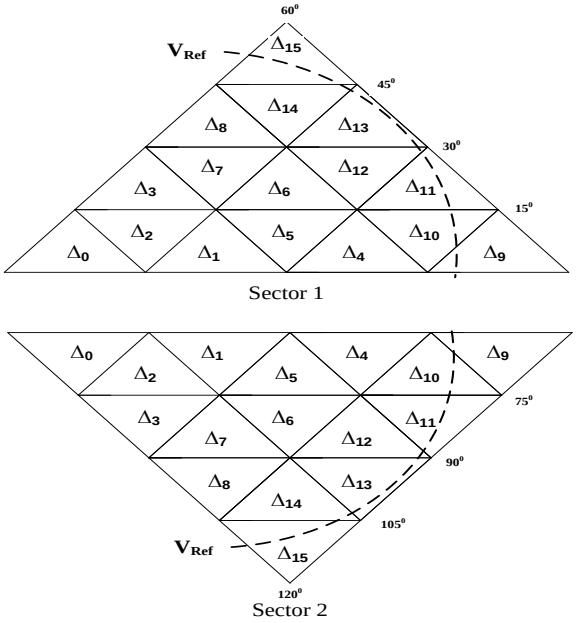

Figure 10: Transition of Reference Vector across Five-Level region in sectors 1 and 2

Sector 1 was extensively used in the analysis of other sectors with a shift in angles as the reference vector rotates beyond sector one while sector 2 and it's like are calculated by the direct reversal of sector 1 with proper placement of angles as the reference vector rotates beyond a given sector. Figure 12 depicts the triangle types and the rotation pattern in a sector.

The angular spacing of 42 sub-triangles of the six sectors of five-level voltage as the reference vector rotates around the triangles of the six sectors are listed as follows:

Sector 1 — 15^0 — 30^0 — 45^0 — 60^0

Sector 2 — 75^0 — 90^0 — 105^0 — 120^0

Sector 3 — 135^0 — 150^0 — 175^0 — 180^0

Sector 4 — 195^0 — 210^0 — 225^0 — 240^0

Sector 5 — 225^0 — 270^0 — 285^0 — 300^0

Sector 6 — 315^0 — 330^0 — 345^0 — 360^0

Figure 11A: Angular Rotation of Reference Vector across the Six Sectors.

Detailed analyses on space vector switching pattern adopted in this work with pertinent to the duty cycle calculation, space vector reference voltage and reference angle calculation were derived from reputable references presented in [16] - [23]. The flow chart presented in fig.11B represents the algorithmic format employed in the realization of this work.

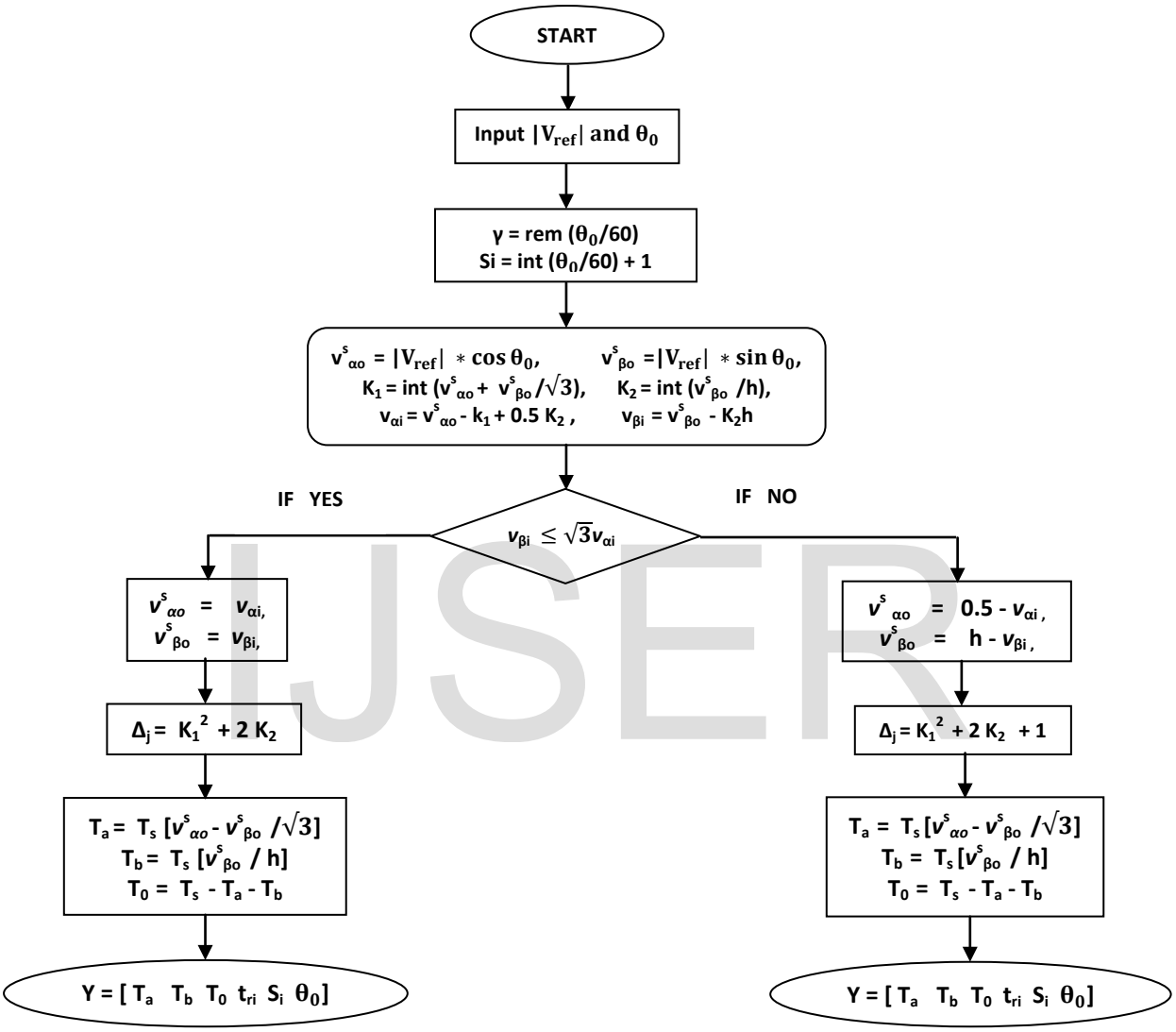

Figure 11B: Flow Chart for Sector Determination and switching on-time.

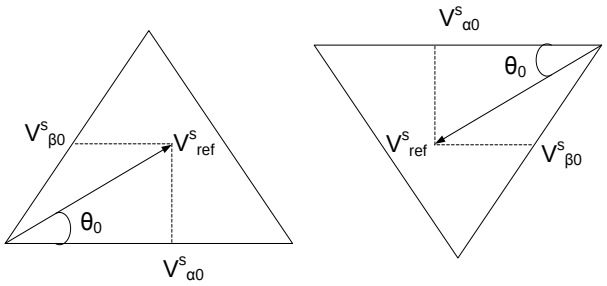

Figure 12: Triangle Types and Rotation Pattern of the Reference Vector in a Sector.
triangle and magnitude Determination.

5.0 SIMULATION RESULTS AND DISCUSSIONS.

Simulation was carried out to determine the inverter output phase and line voltage characteristics with regard to their respective total harmonic distortion using the two techniques of modulations. The results are presented in figures **13-18.** The performance characteristics of the asynchronous machine in terms of speed, torque and current were also verified by the simulation results. The graphical display presented in figures 19 -26, depicts the characteristic behaviour of our proposed studies. During starting, the motor slip is high with low rotor resistance thus drawing much current. When the stator supply voltage is fed directly from the hybrid five-level inverter, the motor starting current increases in magnitude oscillating from -150A to +150A as shown in figure 23 below. Similarly, figure 19 depicts a plot of an externally applied mechanical torque. It is observed from this figure that the rotor accelerates from its starting position with zero value of the applied mechanical torque. Additionally, during motoring operational mode of the machine between 0.75sec.to1.0sec. The applied torque shown in figure 20 dropped from zero to -40NM. This negative value of the applied mechanical torque resulted in a sharp fall in the motor speed as shown in figures 21 and 22 with a rise in the electromechanical torque as presented in figure 20 within a time interval of 0.75sec.to1.0sec. This is in agreement with the inverse characteristics between speed and torque.

In the same vein, at an interval of 1.0sec. to 1.25sec. The value of the applied mechanical torque changed abruptly from -40NM to -20NM which contrastingly resulted in a sharp rise in the motor speed with a concomitant fall in the electromechanical torque. The foregoing analysis indicates that the negative values of the externally applied mechanical torque (-40NM to -20NM and -20NM to -40NM) with a corresponding positive values of the electromechanical torque conforms to the motoring condition of the machine as previously explained in Chee Mong text. Figures 13 and 14 represent the inverter unfiltered phase voltages using SPWM and SVM. It is obviously seen that the output phase voltage of the inverter when modulated by SVM technique increased by 1.15% above the magnitude obtained from SPWM with values of 354Volts for SPWM and 406.85Volts for SVM. Similarly, a corresponding inverter filtered output voltage supplied to the stator terminal of the machine had a good reduction in the percentage harmonic distortion values as depicted in figures 17 and 18 with values of 1.46% for SPWM and 1.06% for SVM as against 34.67% and 30.07% obtained in unfiltered inverter phase output voltage condition. This percentage reduction in harmonics ensured a good efficiency in the machine control and smooth running performance devoid of noise that is associated with harmonics.

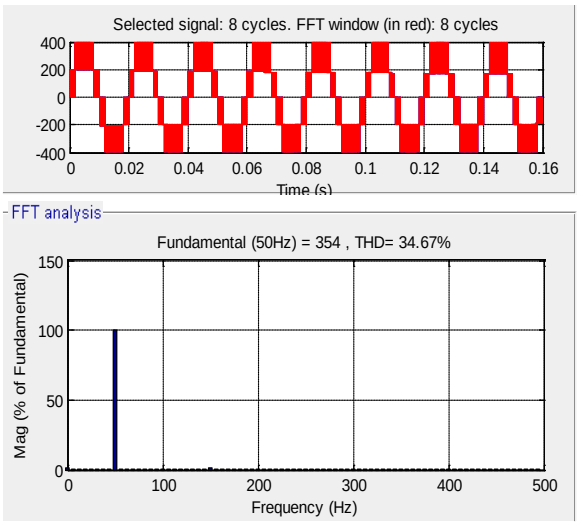

Figure 13: 5level Phase Voltage with SPWM

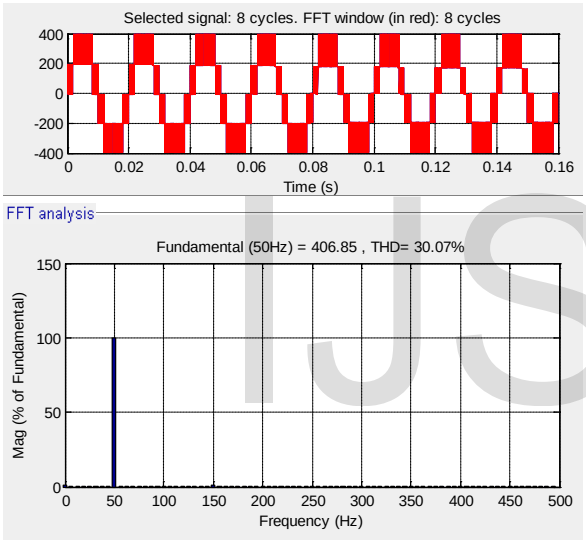

Figure 14: 5level Phase Voltage with SVM

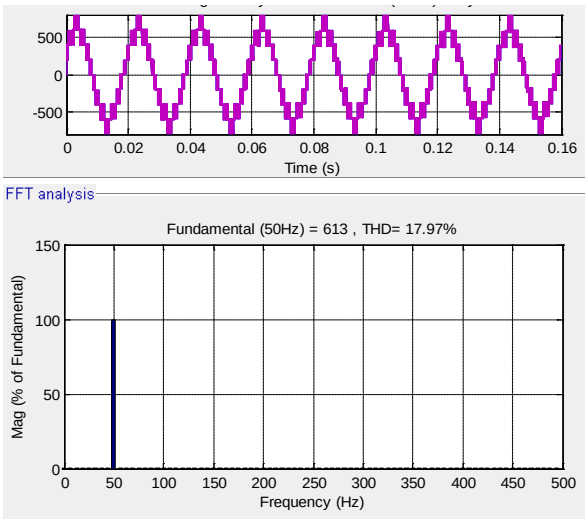

Figure 15: 5level Line Voltage with SPWM

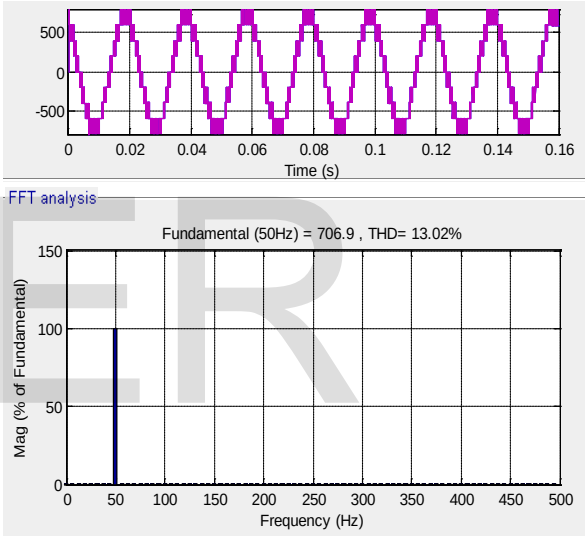

Figure 16: 5level Line Voltage with SVM

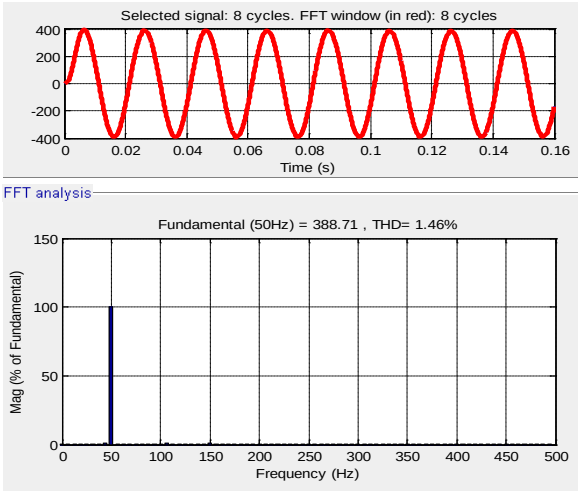

Figure 17: Filtered Phase Voltage with SPWM

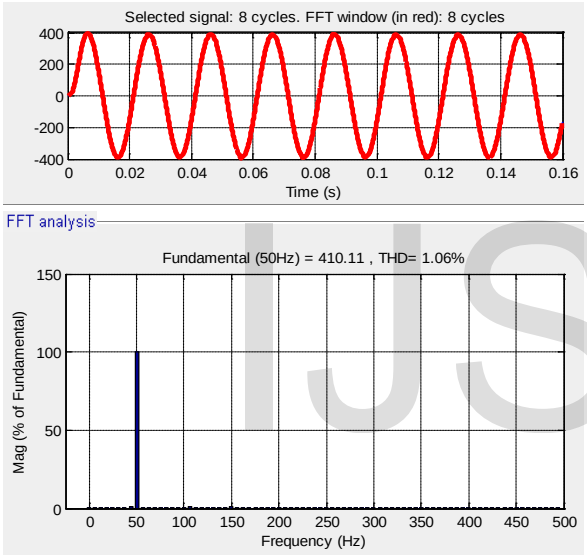

Figure 18: Filtered Phase Voltage with SVM

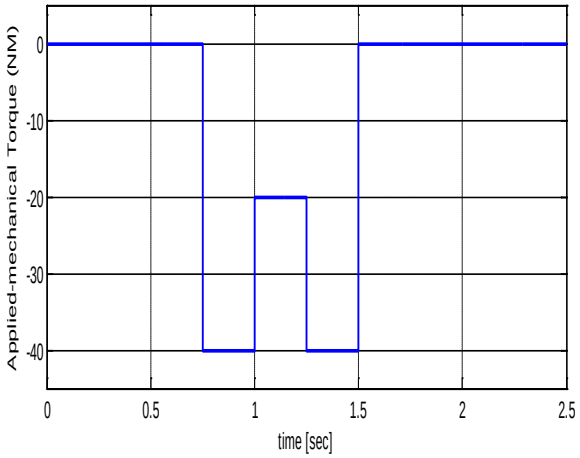

Figure 19: A Plot of Applied-Mechanical Torque against Time.

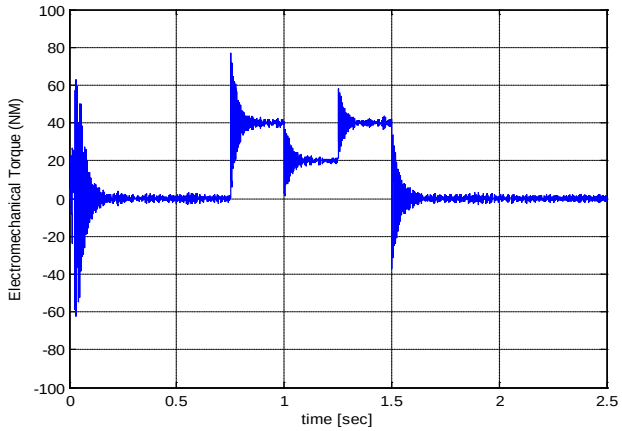

Figure 20: A Plot of Electromechanical Torque against Time.

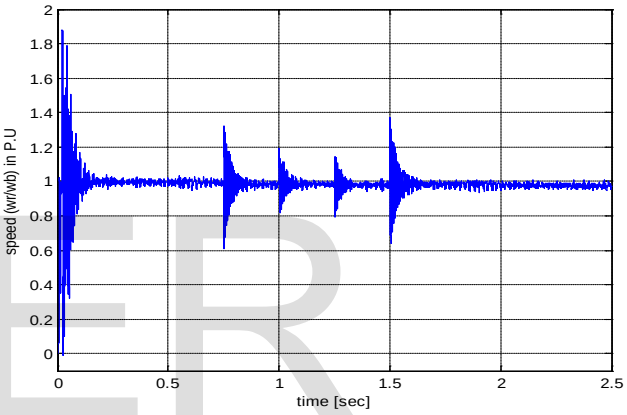

Figure 21: A Plot of per-unit speed ($\frac{\omega_r}{\omega_b}$) against Time.

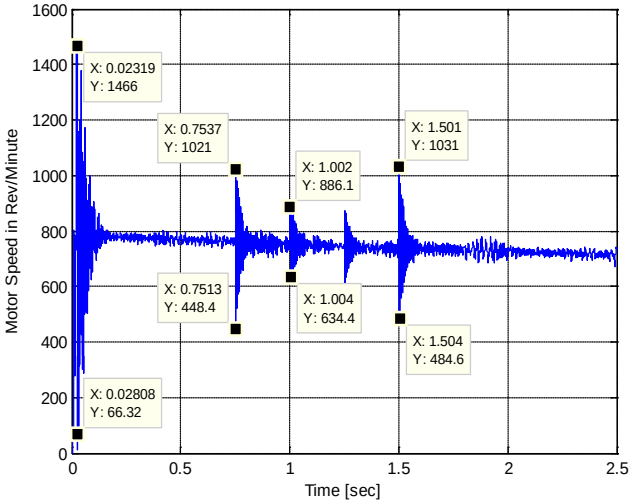

Figure 22: A Plot of Motor Speed (ω_r) against Time.

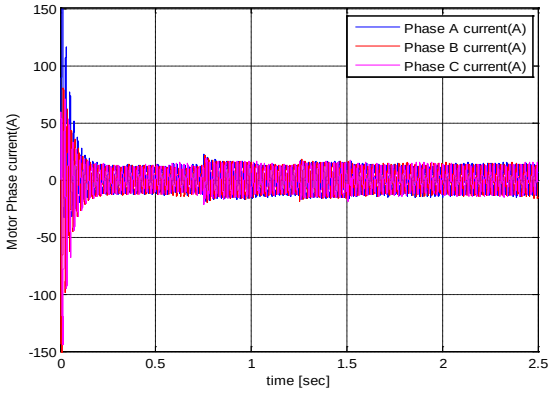

Figure 23: A Plot of three phase currents against Time.

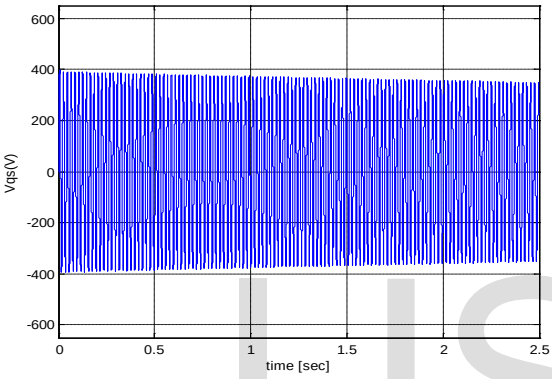

Figure 24: A Plot of Q-axis phase voltage against Time.

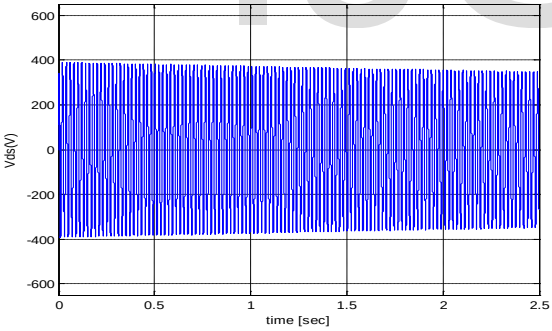

Figure 25: A Plot of D-axis phase voltage against Time.

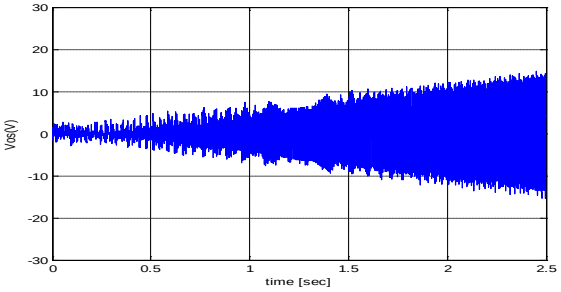

Figure 26: A Plot of zero-axis phase voltage against Time.

6.0 CONCLUSION

The results presented in the above inverter phase and line voltages using multicarrier sinusoidal pulse width modulation and space vector modulation proved that a sufficient magnitude of percentage harmonic distortion is reduced using space vector modulation than the counterpart sinusoidal modulation technique as indicated in their respective THD values. In Fig. 18, 5level converter filtered output phase voltage with SVPWM; the inverter produced a much reduced percentage harmonic distortion value from %THD of 30.07% to 1.06% and generates a good voltage profile of magnitude rising from 406.85v to 410.11v which is fed to the stator winding. This harmonic reduction helps in reducing the rate of reactive losses, undue vibrations, excessive heating and bearing stress inherent in rotor field winding under high harmonics supplied via the stator. This concept was not really considered in the technical reports presented in [8] and [10].

The value of T_{mech} would always be negative for all motoring condition of the induction machine as in the case of an externally applied load torque as shown in figure 19 and will always be positive for the generating condition of the motor just as it is in the case of shaft torque from a prime mover. Contrastingly, T_{em} is always positive for all motoring condition and negative for all generating condition as shown in figure 20. In figure 20 it is obvious that the rise and fall in the torque value agrees with the theory that a change in the externally applied mechanical torque introduces a change in value of the electromechanical torque of the machine as proven in the above simulation result analysis.

7.0 REFERENCES

[1] Krause, P. Wasynczuk, O. and Sudhoff, S.D."Analysis of Electric Machinery," McGraw-Hill Inc, 1986.

[2] Mora, J.F. Electrical Machines**.** McGraw Hill, New York, 2003.

[3] Mohan, N. Undeland, T.M. & Robbins, W.P, Power Electronics Converters,

Applications and Design**,** Wiley and Sons, India, 2nd edition,1995.

[4] Richard, M.C. Electric Drives and Their Control. Oxford University Press: New York, 1995.

[5] Bimbhra, P.S. Power Electronics. Khanna Publishers: New Delhi, India 5th edition, 2012.

[6] Rajeevan, P.P. Sivakumar, K. Chintan. Patel, Ramchand, Rajiv. and Gopakumar, K. "A Seven Level Inverter Topology for Induction Motor Drive Using Two-Level Inverters and Floating Capacitor Fed H-Bridges". IEEE Transactions on Power Electronics, Vol.26 No.6, pp1733-1740, June 2011.

[7] Tekwani, P.N. Kanchan, R.S. and Gopakumar, K. "A dual Five Level Inverter-Fed Induction Motor drive with Common Mode Voltage Elimination and d.c link Capacitor voltage balancing Using only the Switching state redundancy". IEEE Trans. Ind. Electron.,Vol.54, No.5, pp.2600-2608, Oct.2007.

[8] Ogbuka, C.U. "Dynamic Modeling and Simulation of A 3HP Asynchronous Motor Driving A Mechanical Load". Pacific Journal of Science and Technology Vol.10, No.2, pp77-82, 2009.

[9] Modal, G. Sivakumar, K. Ramchand, R. Gopakumar, K. and Levi, E. "A dual Seven Level Inverter Supply for an Open-end Winding Induction Motor Drive, IEEE Trans. Ind. Electron., Vol.56, No.5, pp. 1665-1673, May 2009.

[10] Linga Swamy, R. and Satish Kumar, P. "Speed Control of Space Vector Modulated Inverter Driven Induction Motor". Proceedings of the International MultiConference of Engineers and Computer Scientists Vol.2, IMECS 2008, 19-21 March, 2008. Hong Kong.

[11] Jidin, A. and Sutikno, T. "Matlab/Simulink Based Analysis of Voltage Source Inverter with Space Vector Modulation". TELKOMNIKA, Vol.7 No.1, pp.23-30, April, 2009.

[12] Ong, C.M. Dynamic Simulation of Electric Machinery Using Matlab/Simulink,

Prentice Hall PTR. Upper Saddle River, New Jersey, 1998.

[13] Bose, B.K. "Power Electronics and Motor Drives, Recent Progress and Perspective",

IEEE Transaction on Industrial Electronics, Vol. 56, No.2, pp.581-588, February, 2009.

[14] OMEJE, C.O., Nnadi, D.B and Odeh. C.I. Comparative Analysis of Space Vector Pulse-Width Modulation and Third Harmonic Injected Modulation on Industrial Drives,

Pacific Journal of Science and Technology, Vol.13, No.1 pp.12-19, 2012.

[15] Govindaraju, C. and Baskaran, K. "Efficient Hybrid Carrier Based Space Vector Modulation for Cascaded Multi-Level Inverter," Journal on Power Electronics,

Vol.10 No.3, pp. 277-284, May 2010.

[16] Gupta, A.K. and Khambadkone, A.M. A General Space Vector PWM Algorithm for Multi-Level Inverters, Including Operation in Over-Modulation Range, IEEE Transactions on Power Electronics, (Vol.22, No.2, PP.518-519, March, 2007.

[17] Gupta, A.K. and Khambadkone, A.M, A Space Vector PWM Scheme for Multi-Level Inverters Based on Two-Level Space Vector PWM, IEEE Transactions on industrial Electronics, (Vol.53, No.5, PP.1633-1634, October, 2006.

[18]. OMEJE, C.O. Odeh, C.I. Nnadi, D.B. Agu, M.U. & Obe, E.S**,** Space Vector Pulse Width

Modulation of A Multi-Level Diode Clamped Converter with Experimental Verification

Nigerian Journal of Technology, Vol. 30, No. 2, June 2011.

[19] Holmes, D.G. and Lipo, T.A. Pulse width Modulation for Power Converters Principles and Practice**,** IEEE Press / Wiley- Interscience, New York, 2003.

[20] Holmes D.G**,** The General Relationship between Regular- Sampled Pulse width

Modulation and Space Vector Modulation for Hard Switched Converters, in conf. Rec. IEEE- IAS Annual Meeting, PP.2482-2488, June, 2000.

[21] Saeedifard, M. Nikkhajoei, H. Iravani, R. and Bakhshai, A. "A Space Vector Modulation Approach for A Multi-Module HVDC Converter System", IEEE Transactions on Power Delivery, Vol.22, No.3, pp.1643-1654, July, 2007.

[22] Rodriguez, J. Lai, J.S. and Peng, F.Z. "Multi-Level Inverters: A Survey of Topologies, Controls and Applications", IEEE Transaction on Industrial Electronics, Vol. 49, No.4, pp.724-738, August, 2002.

[23] Kolar, J.W. Friedli, T. Rodriguez, J. and Wheeler, P. "Review of Three-Phase PWM ac-ac converter topologies", IEEE Trans. Industrial Electronic, Vol.58, no.11, pp.4988-5006, Nov.2011.

AUTHOR'S BIOGRAPHY

OMEJE, Crescent Onyebuchi obtained his B.Eng. (Electrical Engineering) in 2004 and M.Eng. (Power Electronics and Drives) in 2011 from the University of Nigeria, Nsukka. He is a member Nigerian Institute of Electrical and Electronic Engineering. He is COREN registered and currently a Ph.D student in University of Nigeria, Nsukka. He is a full time lecturer in the Department of Electrical/Electronic Engineering, University of Port Harcourt, Rivers State, Nigeria. His research interests are centered on renewable energy, power electronics converters applications and drives.